View metadata, citation and similar papers at core.ac.uk
brought to you by CORE
provided by Bilkent University Institutional Repository

Phys. Status Solidi A **209,** No. 6, 1119–1123 (2012) / **DOI** 10.1002/pssa.201127416

physica status solidi a
www.pss-a.com
applications and materials science

Magnetotransport study on AlInN/(GaN)/AlN/GaN heterostructures

Aydın Bayraklı[*,1,2], Engin Arslan[,3], Tezer Fırat[1], Şadan Özcan[1], Özgür Kazar[3], Hüseyin Çakmak[3], and Ekmel Özbay[3,4]**

[1] Faculty of Engineering, Department of Physics Engineering, Hacettepe University, 06800 Ankara, Turkey
[2] Undersecretariate for Defence Industries (SSM), Balgat, 06520 Ankara, Turkey
[3] Nanotechnology Research Center-NANOTAM, Bilkent University, 06800 Ankara, Turkey
[4] Departments of Physics and Electrical and Electronics Engineering, Bilkent University, 06800 Ankara, Turkey

Received 18 July 2011, revised 5 December 2011, accepted 30 January 2012
Published online 27 February 2012

Keywords GaN, heterostructures, magnetotransport

[*] Corresponding author: e-mail abayrakl@ssm.gov.tr, Phone: +90 312 411 92 43, Fax: +90 312 411 93 86
[**] e-mail engina@bilkent.edu.tr, Phone: +90 312 290 10 20, Fax: +90 312 290 10 15

We report the effect of a thin GaN (2 nm) interlayer on the magnetotransport properties of AlInN/AlN/GaN-based heterostructures. Two samples were prepared (Sample A: AlInN/AlN/GaN and sample B: AlInN/GaN/AlN/GaN). Van der Pauw and Hall measurements were performed in the 1.9–300 K temperature range. While the Hall mobilities were similar at room temperature (RT), sample B had nearly twice as large Hall mobility as sample A at the lowest temperature; 679 and 889 cm^2/Vs at RT and 1460 and 3082 cm^2/Vs at 1.9 K for samples A and B. At 1.9–10 K, the longitudinal magnetoresistance was measured up to 9 T, in turn revealing Shubnikov–de Haas (SdH) oscillations. The carrier concentration, effective mass and quantum mobility of the two-dimensional electron gas (2DEG) were determined from SdH oscillations. At 1.9 K, the 2DEG concentration of sample B was nearly seven times larger than of sample A (1.67×10^{13}/cm^2 vs. 0.24×10^{13}/cm^2). On the contrary, the quantum mobility was changed adversely nearly three times (sample B 2500 cm^2/Vs and sample A 970 cm^2/Vs). The increase of the 2DEG concentration was attributed to the existence of the GaN interlayer, which has strengthened the spontaneous polarization difference between the AlInN and GaN layers of the heterostructure. Hence, the stronger electric field at the 2DEG region bent the conduction band profile downwards and consequently the quantum mobility decreased due to the increased interface roughness scattering.

© 2012 WILEY-VCH Verlag GmbH & Co. KGaA, Weinheim

1 General In recent years, high quality AlInN/GaN-based heterostructures joined the III-nitride family research activities with higher sheet concentration than AlGaN/GaN [1–4]. Hence, the optimal lattice-match of the AlInN alloy to GaN is suggested at around 18% indium [5–7]. Furthermore, it is reported that sheet concentration and mobility are variable with the AlN interlayer thickness that is maximal at different AlN thicknesses. This behaviour requires a trade-off between the electron concentration and transport mobility (between the power and frequency requirements of a transistor device). Typical room temperature (RT) values for the achieved Hall mobilities of lattice-matched AlInN/AlN/GaN heterostructures are reported as follows; 1170 cm^2/Vs ($n_H = 2.55 \times 10^{13}$/$cm^2$) at 1.1 nm AlN [8], 1510 cm^2/Vs ($n_H = 1.16 \times 10^{13}$/$cm^2$) at 1 nm AlN [9] and 1630 cm^2/Vs ($n_H = 1.20 \times 10^{13}$/$cm^2$) at 1 nm AlN [10] promising future interest on AlInN/AlN/GaN.

In this study, in addition to the optimal AlN interlayer, the effect of a thin 2 nm GaN interlayer on the magnetotransport properties of an AlInN/AlN/GaN heterostructure has been investigated. Two samples were prepared by exactly the same conditions except the GaN interlayer, AlInN/AlN/GaN (sample A) and AlInN/GaN/AlN/GaN (sample B), respectively.

2 Samples The $Al_{1-x}In_xN$/(GaN)/AlN/GaN ($x = 0.17$) heterostructures were grown on a *c*-plane (0001) Al_2O_3 substrate by a low-pressure metalorganic chemical-vapour deposition (MOCVD) reactor. Prior to the epitaxial growth, the Al_2O_3 substrate was annealed at 1100 °C for 10 min in

© 2012 WILEY-VCH Verlag GmbH & Co. KGaA, Weinheim

order to remove surface contamination. The growth was initiated with a 15 nm thick low-temperature (840 °C) AlN nucleation layer. Then, a 320 nm high-temperature (HT) AlN buffer layer (BL) was grown at a temperature of 1150 °C. A 1160 nm thick undoped GaN BL was then grown at 1070 °C and a reactor pressure of 200 mbar. Above the GaN BL, a 2 nm thick HT-AlN layer was grown at 1085 °C with a pressure of 50 mbar. For sample A, the HT-AlN layer was followed by a 17 nm thick AlInN ternary layer. For sample B, the HT-AlN layer was followed first by a 2 nm GaN interlayer (at 1070 °C and 200 mbar), and then by a 17 nm thick AlInN ternary layer. The AlInN ternary layer was grown at 800 °C and a pressure of 50 mbar. Finally, a 3 nm thick GaN cap layer growth was carried out at a temperature of 1085 °C and a pressure of 50 mbar for both samples. The schematic representations of the samples are given below in Fig. 1.

The grown wafers were cut into several pieces and the ohmic contacts were formed as Van der Pauw (square shaped) geometry with the dimensions 5 mm × 5 mm in the high vacuum coating system at approx. 10^{-7} Torr. Prior to ohmic contact formation, the samples were cleaned with acetone in an ultrasonic bath. Then, the samples were treated with boiling isopropyl alcohol for 5 min and rinsed in de-ionized (DI) water that possessed 18 MΩ resistivity. After cleaning, the samples were dipped in a solution of HCl/H_2O (1:2) for 30 s in order to remove the surface oxides, and were then rinsed in DI water again for a prolonged period. Ti/Al/Ni/Au (16/180/50/150 nm) metals were thermally evaporated on the sample and were annealed at 700 °C for 30 s in N_2 ambient in order to form the ohmic contact.

3 Measurements Measurements were performed using van der Pauw and Hall techniques at a temperature range 1.9–300 K. The current was chosen as 100 μA, which was meant for a low electric field (<0.05 V/cm) in order to prevent joule heating. The applied magnetic field was 0.5 T and it was perpendicular to the sample surface. The measured sheet resistance (R_S), sheet carrier density (n_H) and Hall mobility (μ_H) versus temperature are summarized for specific temperatures in Table 1. Sample A has close values

(a)

GaN Cap Layer	3 nm
AlInN Layer	17nm
AlN Spike Layer	2 nm
ud-GaN Layer	1160 nm
HT AlN Buffer Layer	320 nm
AlN NL	15nm

(b)

GaN Cap Layer	3 nm
AlInN Layer	17 nm
GaN Layer	2 nm
AlN Spike Layer	2 nm
ud-GaN Layer	1160 nm
HT AlN Buffer Layer	320 nm
AlN NL	15nm

Figure 1 Schematic view of the samples (a) sample A: AlInN/AlN/GaN and (b) sample B: AlInN/GaN/AlN/GaN with 2 nm GaN interlayer.

Table 1 Sheet resistance (R_S), sheet carrier density (n_H) and Hall mobility (μ_H) found by Van der Pauw and Hall measurements at 1.9, 77 and 300 K.

sample	R_S (Ω/sqr)			n_H (10^{13}/cm^2)			μ_H (cm^2/Vs)		
	1.9 K	77 K	300 K	1.9 K	77 K	300 K	1.9 K	77 K	300 K
A	140	143	276	3.06	3.07	3.33	1460	1419	679
B	72	76	237	2.81	2.84	2.95	3082	2901	889

with those reported in the literature for AlInN/AlN/GaN heterostructures with similar AlN layer thicknesses [8–10]. Sample B has also similar values. However, it has lower R_S and higher μ_H at all temperatures. At 1.9 K, μ_H of sample B increased up to twice the value of sample A. Conversely, sample B had always lower n_H, whereas n_H did not change significantly with temperature for both samples.

The measurements indicate that the GaN interlayer has an effect on the magnetotransport properties of the AlInN/GaN/AlN/GaN heterostructure and is, therefore, interesting for research. Nevertheless, none of these measurements give any information evidently about the two-dimensional electron gas (2DEG) existing at the AlN/GaN interface. One way of studying the 2DEG concentration and transport mobility here could be working on the temperature dependence of the Hall measurements at low and high magnetic fields, which can be used to separate the 2DEG electron concentration from the remaining bulky electrons of the heterostructure (GaN side of AlN/GaN) [11, 12]. In this study, the longitudinal magnetoresistance measurements were carried out looking for Shubnikov–de Haas (SdH) oscillations which are directly related with 2DEG concentration and quantum mobility of the 2D electrons.

In the 1.9–10 K temperature range, the longitudinal magnetoresistance (R_{xx}) was measured up to 9 T magnetic field. The applied current 100 μA was low enough not to heat the 2DEG in both samples to observe SdH oscillations clearly. The measurements are plotted in Fig. 2. For sample

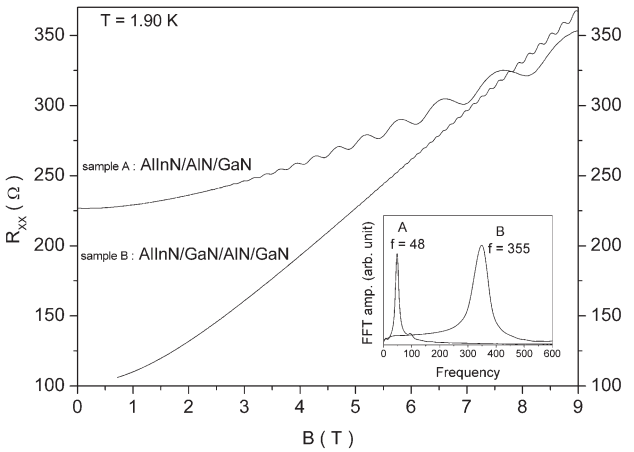

Figure 2 The longitudinal magnetoresistance (R_{xx}) and oscillatory behaviour (SdH oscillations) at 1.9 K for samples A and B. The inset shows the FFT frequencies of the oscillations.

© 2012 WILEY-VCH Verlag GmbH & Co. KGaA, Weinheim

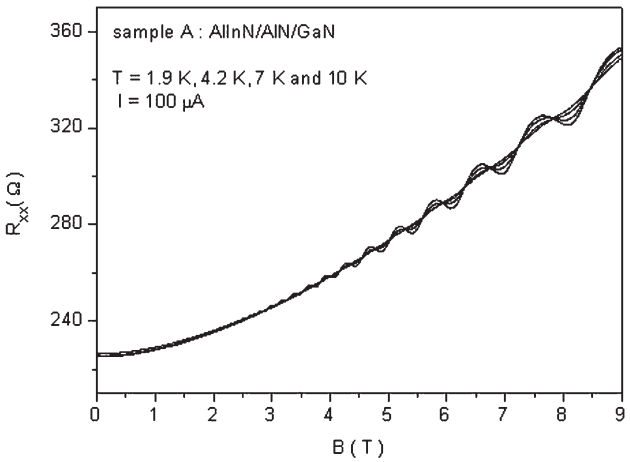

Figure 3 Temperature dependence of longitudinal magnetoresistance measured at 1.9, 4.2, 7.0 and 10.0 K for sample A. The oscillatory behaviour decreases with increasing temperature.

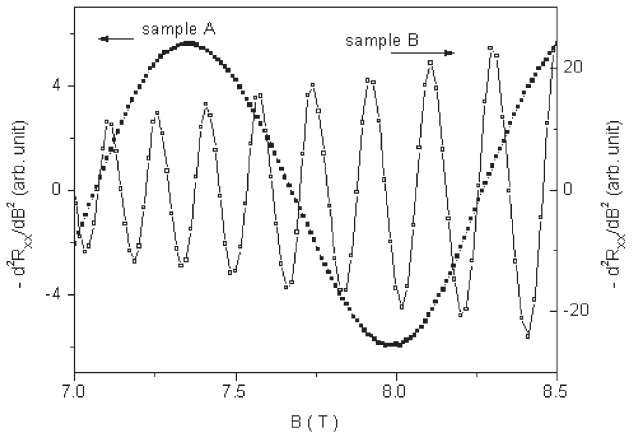

Figure 4 SdH oscillations obtained by taking the 'minus second derivative' of the longitudinal magnetoresistance (R_{xx}) with respect to magnetic field.

A, the SdH oscillations were observable starting from magnetic fields of 3 T. For sample B with the GaN interlayer, the oscillations started after 6 T. SdH oscillations were observable for both samples up to 10 K. As an example, the temperature dependence of SdH oscillations for sample A is shown in Fig. 3.

Before starting the analysis, SdH oscillations (the oscillatory term) have to be carefully extracted from the measured longitudinal magnetoresistance data using various techniques; such as smoothing, interpolating to equally spaced data with respect to the inverse magnetic field ($1/B$), and taking the derivatives with respect to B. Finally, the second derivative gives the oscillatory term with the periodicity $\Delta(1/B)$ as shown in Fig. 4.

The 2D electron concentration (n_{2D}) related to the period of the SdH oscillations is [13]

$$n_{2D} = \frac{e}{\pi\hbar\Delta\left(\frac{1}{B_n}\right)}, \tag{1}$$

where $\Delta(1/B_n)$ is the period of the oscillations and B_n ($n = 1, 2, 3\ldots$ etc.) corresponds to the magnetic fields of successive peaks, e is the electron charge and $\hbar$ is Planck's constant divided by 2π. Respectively, from the SdH data, the slope in Fig. 5 is equal to $\Delta(1/B)$ and using Eq. (1) n_{2D} is found as: 0.24×10^{13} and $1.67 \times 10^{13}/\mathrm{cm}^2$ for samples A and B. For consistency, frequency analysis was performed using the fast Fourier transform (FFT) technique on SdH data. The FFT results point towards one dominant frequency for each sample, which is shown as an inset in Fig. 2. Therefore, only the lowest subband in the 2DEG region is occupied for both samples.

From the temperature dependence of the amplitudes of SdH oscillations, the effective mass of 2D electrons (m^*) can

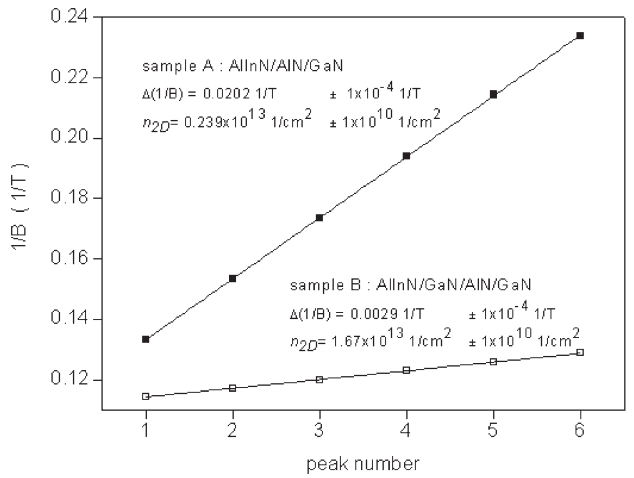

Figure 5 $1/B$ versus successive peaks. 2DEG concentration is found from the best fits of Eq. (1) to the plotted data.

be found using [14]

$$\frac{A(T, B_n)}{A(T_0, B_n)} = \frac{T \sin h(2\pi^2 k_B T_0 m^*/\hbar eB)}{T_0 \sin h(2\pi^2 k_B T m^*/\hbar eB)}, \tag{2}$$

where $A(T, B_n)$ and $A(T_0, B_n)$ are the SdH amplitudes at temperatures T and T_0 (1.9 K, the lowest temperature) at magnetic field B_n of the n-th peak and k_B is the Boltzmann constant. Figure 6 shows the temperature dependence of the relative amplitudes ($A(T, B_n)/A(T_0, B_n)$). From the best fit to Eq. (2) as plotted in Fig. 6, m^* was found $0.25\, m_e \pm 0.01\, m_e$ for both samples and goes with those reported for GaN-based heterostructures [15, 16].

Once, the effective mass was found, the quantum mobility μq can be determined from the magnetic field

© 2012 WILEY-VCH Verlag GmbH & Co. KGaA, Weinheim

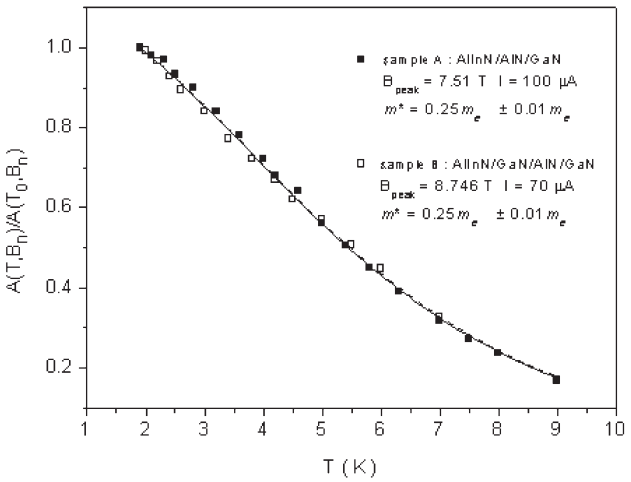

Figure 6 Temperature dependence of the relative SdH amplitudes. 2D electron effective mass is found from the best fit of Eq. (2) to the plotted data.

dependence of the SdH amplitudes using [14]

$$\ln\left[\frac{A(T,B_n)B_n^{-1/2}\sin h\,\chi}{\chi}\right] = (\text{const.}) - \frac{\pi}{\mu_q}\frac{1}{B_n}, \qquad (3)$$

$$\chi = \frac{2\pi^2 k_B T_0 m^*}{\hbar e B_n}, \qquad (4)$$

Correspondingly, Fig. 7 shows best fits of Eq. (3) (Dingle plots) for samples A and B.

4 Discussion n_H and μ_H, n_{2D} and μq obtained from Van der Pauw, Hall, and SdH measurements at 1.9 K are summarized in Table 2. From the comparison of sheet carrier densities with 2DEG concentrations, we can state that both samples show parallel conduction; sample A with $n_H = 3.06 \times 10^{13}/\text{cm}^2$ and $n_{2DEG} = 0.24 \times 10^{13}/\text{cm}^2$ has less electrons in 2DEG channel than sample B with a 2 nm GaN interlayer with $n_H = 2.81 \times 10^{13}/\text{cm}^2$ and $n_{2DEG} = 1.67 \times 10^{13}/\text{cm}^2$.

For the AlInN/AlN/GaN heterostructure, the spontaneous polarization difference between AlInN and GaN is known as the major cause of the 2DEG concentration [3, 7]. Our result, argues that introducing a thin GaN layer strengthens the polarization difference and, therefore, increases the electric field at the interface and causes a further increase of 2DEG concentration.

For the 2DEG mobility results, the scattering processes are in the scene. The main scattering mechanisms at low temperatures are alloy disorder, interface roughness, background impurity and acoustic phonon [10]. The alloy disorder scattering is largely reduced by the insertion of an AlN interlayer into the structure that is valid for both samples. The GaN interlayer can be suggested for the further

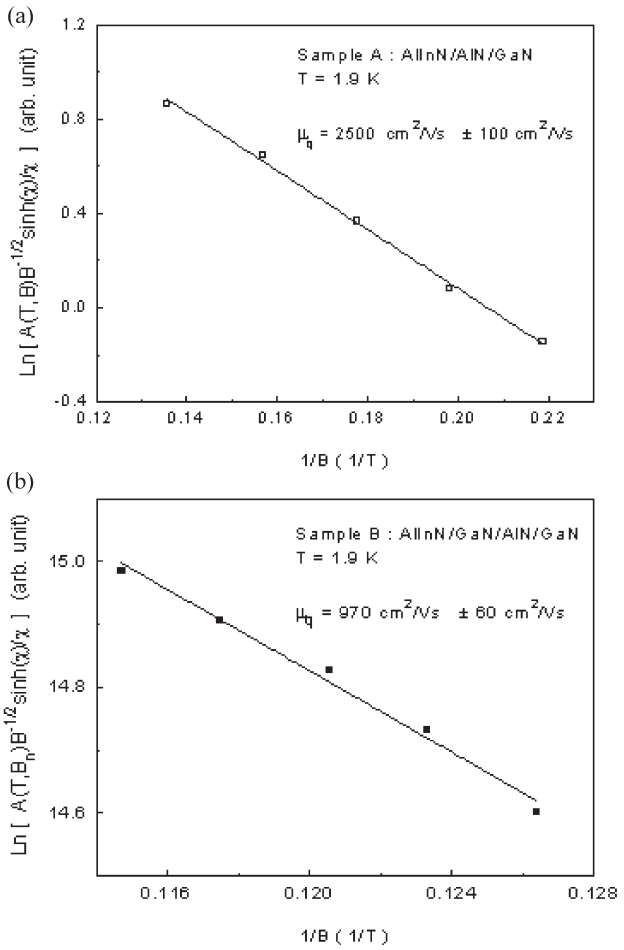

Figure 7 Determination of the quantum mobility μq. The lines represent the best fits of Eq. (3) to the plotted data: (a) for sample A and (b) for sample B.

decrease of the alloy scattering for sample B. Due to the increase of screening effect corresponding to the increased 2DEG density, the impurity and phonon scattering cannot the reason of lower quantum mobility for sample B. In addition, impurity and phonon scattering is not affected by the distance of 2DEG from the interface [10, 17]. However, the interface roughness scattering is dependent on the distance of 2DEG from the interface. In our case, only the first sub-band was occupied for both samples. For triangular quantum

Table 2 Comparison of the sheet carrier density (n_H) and Hall mobility (μ_H), which were found by Van der Pauw and Hall measurements with 2DEG concentration (n_{2DEG}) and quantum mobility (μq), which were found from SdH data. Measurements were collected at 1.9 K.

sample	n_H ($10^{13}/\text{cm}^2$)	n_{2DEG} ($10^{13}/\text{cm}^2$)	μ_H (cm^2/Vs)	μ_q (cm^2/Vs)
A	3.06	0.24	1460	2500
B	2.81	1.67	3082	970

© 2012 WILEY-VCH Verlag GmbH & Co. KGaA, Weinheim

wells, lower sub-bands are reported as closer to the interface; and therefore, are expected with smaller scattering times (lower quantum mobility) [17]. Thus, it is suggested that Sample B with the influence of greater polarization difference has bent the conduction band profile deeper at the interface so that the first sub-band (the only occupied sub-band) was closer to the interface and consequently the interface roughness scattering occurred more intensively with respect to Sample B. The quantum mobility is associated with 2D electrons only. But, when compared at sample level, the measured Hall mobility is increased due to decreased number of low mobility electrons on the bulk GaN side. Hence, for quantitative results, a parallel conduction analysis is required to separate the transport mobilities (2D and 3D) and carrier concentrations (2D and 3D) of each sample individually.

In conclusion, it is suggested that a thin GaN interlayer has noteworthy effects on the magnetotransport properties of AlInN/AlN/GaN heterostructures and, therefore, is proposed for further studies.

Acknowledgements This work was supported by the projects DPT-HAMIT, EU-PHOME, EU-N4E, NATO-SET-181 and TUBITAK under Project Nos., 107A004, 107A012, 109E301. One of the authors (E. Ö.) also acknowledges partial support from the Turkish Academy of Sciences.

References

[1] S. Yamaguchi, M. Kariya, S. Nitta, H. Kato, T. Takeuchi, C. Wetzel, H. Amano, and I. Akasaki, J. Cryst. Growth **195**, 309 (1998).
[2] J. Kuzmik, IEEE Electron Device Lett. **22**, 510 (2001).
[3] S. Yamaguchi, M. Kosaki, Y. Watanabe, S. Mochizuki, T. Nakamura, Y. Yukawa, S. Nitta, H. Amano, and I. Akasaki, Phys. Status Solidi A **188**, 895 (2001).
[4] J. F. Carlin and M. Ilegems, Appl. Phys. Lett. **83**, 668 (2003).
[5] J. F. Carlin, C. Zellweger, J. Dorsaz, S. Nicolay, G. Christmann, E. Feltin, R. Butté, and N. Grandjean, Phys. Status Solidi B **242**, 2326 (2005).
[6] K. Lorenz, N. Franco, E. Alves, I. M. Watson, R. W. Martin, and K. P. O'donnell, Phys. Rev. Lett. **97**, 085501 (2006).
[7] C. Hums, J. Bläsing, A. Dadgar, A. Diez, T. Hempel, J. Christen, and A. Krost, Appl. Phys. Lett. **90**, 022105 (2007).
[8] M. Gonschorek, J. F. Carlin, E. Feltin, M. A. Py, and N. Grandjean, Appl. Phys. Lett. **89**, 062106 (2006).
[9] J. Xie, X. Ni, M. Wu, J. H. Leach, Ü. Özgür, and H. Morkoç, Appl. Phys. Lett. **91**, 132116 (2007).
[10] A. Teke, S. Gökden, R. Tülek, J. H. Leach, Q. Fan, J. Xie, Ü. Özgür, H. Morkoç, S. B. Lisesivdin, and E. Özbay, New J. Phys. **11**, 063031 (2009).
[11] S. B. Lisesivdin, N. Balkan, and E. Özbay, Microelectron. J. **40**, 413 (2009).
[12] A. Yıldız, S. B. Lisesivdin, M. Kasap, S. Özçelik, E. Özbay, and N. Balkan, Appl. Phys. A **98**, 557 (2010).
[13] W. De Lange, Ph.D. Thesis (Eindhoven University of Technology, The Netherlands, 1993).
[14] N. Balkan, N H. Çelik, A. J. Vickers, and M. Cankurtaran, Phys. Rev. B **52**, 17210 (1995).
[15] S. Elhamri, R. Newrock, D. Mast, M. Ahoujja, W. Mitchel, J. Redwing, M. Tischler, and J. Flynn, Phys. Rev. B **57**, 1374 (1998).
[16] T. Wang, J. Bai, S. Sakai, Y. Ohno, and H. Ohno, Appl. Phys. Lett. **76**, 2737 (2000).
[17] Z. L. Miao, N. Tang, F. J. Xu, L. B. Cen, K. Han, J. Song, C. C. Huang, T. J. Yu, Z. J. Yang, X. Q. Wang, G. Y. Zhang, B. Shen, K. Wei, J. Huang, and X. Y. Liu, J. Appl. Phys. **109**, 016102 (2011).

© 2012 WILEY-VCH Verlag GmbH & Co. KGaA, Weinheim